Letter

Examination of the sensitivity of quasifree reactions to details of the bound-state overlap functions

C. A. Bertulani

Department of Physics and Astronomy, Texas A&M University—Commerce, Commerce, Texas 75429-3011, USA
and Institut für Kernphysik, Technische Universität Darmstadt, D-64289 Darmstadt, Germany

A. Idini

Division of Mathematical Physics, Department of Physics, LTH, Lund University, P.O. Box 118, S-22100 Lund, Sweden

C. Barbieri

Dipartimento di Fisica, Università degli Studi di Milano, Via Celoria 16, 20133 Milano, Italy;
INFN, Sezione di Milano, Via Celoria 16, 20133 Milano, Italy;
and Department of Physics, University of Surrey, Guildford GU2 7XH, United Kingdom

It is often stated that heavy-ion nucleon knockout reactions are mostly sensitive to the tails of the bound-state wave functions. In contrast, $(p, 2p)$ and (p, pn) reactions are known to access information on the full overlap functions within the nucleus. We analyze the oxygen isotopic chain and explore the differences between single-particle wave functions generated with potential models, used in the experimental analysis of knockout reactions, and *ab initio* computations from self-consistent Green's function theory. Contrary to common belief, we find that not only the tail of the overlap functions, but also their internal part is assessed in both reaction mechanisms, which are crucial to yield accurately determined spectroscopic information.

Introduction. High-energy ($\gtrsim 100$ MeV/nucleon) neutron and proton removal (knockout) reactions with, e.g., ^{9}Be and ^{12}C targets are one of the most successful tools to investigate the single-particle structure of the many-body wave functions of nuclei far from stability. A large number of experiments yielded an enormous amount of knowledge collected on magicity, shell evolution, two- and three-body halo configurations, spectroscopy of deep-lying states, etc. The magnitude of the knockout cross sections, as well as the momentum distribution of the fragments, has been the main source of information since the very beginning of this experimental campaign [1–3]. Theories have been developed for a credible description of the experimental data [4–8].

It is widely considered that knockout reactions are peripheral and probe the tail of the nucleon removal wave function, due to absorption at low impact parameters (see, e.g., Refs. [9–12]). The removal wave function is given by the overlap integral $I(r) = \langle \Psi_i^{A-1} | \psi(r) | \Psi_{\text{g.s.}}^A \rangle$, where $|\Psi_{\text{g.s.}}^A\rangle$ and $|\Psi_i^{A-1}\rangle$, respectively, denote the (many-body) wave functions for the projectile and the residual fragment in its ith excited state [13,14]. The operator $\psi(r)$ removes a nucleon at position r. The tail of $I(r)$ is proportional to the Whittaker function,

$$I(r) = \langle \Psi_i^{A-1} | \psi(r) | \Psi_{\text{g.s.}}^A \rangle \xrightarrow[r \to \infty]{} C \frac{1}{r} W_{-\eta, l+1/2}(2\kappa r), \quad (1)$$

where $\kappa = \sqrt{2\mu E_B}/\hbar$ is the wave number, μ the reduced mass between the outgoing nucleon and the $(A - 1)$ residual, E_B is the removed nucleon separation energy, $\eta = \mu Z_N Z_{(A-1)} e^2 / \hbar \kappa$

is the Coulomb parameter, with Z_A and Z_N the target and projectile charges, and l is the angular momentum of the removed nucleon.

Eikonal models for knockout reactions [4–12,15] imply that the total knockout cross section is proportional to the integral of the square $I^2(r)$ and, as long as the reaction is truly peripheral, to the squared asymptotic normalization coefficient (ANC): C^2. In this case the ANC is the only messenger carrying information about the complex many-body wave functions $|\Psi_{\text{g.s.}}^A\rangle$ and $|\Psi_k^{A-1}\rangle$ entering Eq. (1). *Ab initio* methods compute the shape of overlap functions microscopically, even where these are not well represented by mean-field orbits. Moreover, they can handle the large model spaces necessary to resolve the *full* quenching of spectroscopic factors due to correlations [16]. In contrast, phenomenological assumptions on radial shapes cannot be avoided even for long-used approaches such as the shell model [17,18]. In practice, most applications in the literature still assume that the tail of $I(r)$ does not differ from an independent-particle approximation (IPA) wave function, for example, a Woods-Saxon (WS) plus spin orbit tuned to the corresponding separation energy. Compared to the experimental data on nucleon knockout reactions, the square of C can be extracted and compared to predictions of many-body models (e.g., shell-model calculations). This procedure is used to determine the spectroscopic factors S according to [15,19]

$$C_{\text{exp}}^2 = S \cdot C_{\text{IPA}}^2, \quad (2)$$

where $C_{\rm IPA}$ is computed assuming that its IPA wave function is properly normalized to unity.[1] Nuclear correlations have the effect of quenching the spectroscopic factor, $S \equiv \int I^2(r) \, d^3r$, and so the experimental value of $C_{\rm exp}$ is smaller than its IPA. The many-body ANC, $C_{\rm MB}$, computed through Eq. (1) should be compared directly to $C_{\rm exp}$. The primary goal of nucleon knockout experiments with heavy-ion targets is to extract information on the spectroscopic factors and the $C_{\rm MB}$.

New experiments have been carried out or are planned using (p, pN), with $N = p, n$, reactions in inverse kinematics [20–23]. New reaction models have been developed differing from those appropriate for knockout reactions with heavy targets [24,25]. The proton probes are more sensitive to the inner parts of the nuclear wave function, especially for light nuclear projectiles [21]. Since both knockout as well as (p, pN) reactions are notable spectroscopic tools of unstable nuclei, it is imperative to understand to what extent experimental conclusions can be affected by assumptions in modeling $I(r)$.

Overlaps with ab initio *methods.* The *ab initio* overlaps have been calculated from the Hamiltonian

$$H(A) = T - T_{\rm c.m.}^{[A-1]} + V + W, \qquad (3)$$

where $T_{\rm c.m.}^{[A-1]}$ is the intrinsic kinetic energy for the recoiling system of mass $A - 1$ nucleons, while V and W are the two- and three-body interactions. This formulation is conveniently suited for the calculation of overlap functions and the corresponding nucleon separation energies, E_h [26]. The three-body term W is reduced to an effective two-body operator as outlined in [27]. We used self-consistent Green's function (SCGF) theory within the third-order algebraic diagrammatic construction [ADC(3)] truncation scheme, which accounts for all $2p1h$, $2h1p$ intermediate-state configurations [28,29]. The SCGF self-energy was obtained in a harmonic oscillator basis including 14 major shells ($N_{\rm max} = 13$) and at frequency $\hbar\Omega = 20$ MeV. The correct asymptotic tail of our *ab initio* overlap $I_{\rm GF}^{lj}(r)$ is ensured by a final Dyson diagonalization in the full (nontruncated) momentum space [30],

$$\left[E_h - \frac{k^2}{2\mu} \right] \tilde{I}_{\rm GF}^{lj}(k) = \int dq \, q^2 \, \Sigma^{\star lj}(k, q; E_h) \, \tilde{I}_{\rm GF}^{lj}(q), \qquad (4)$$

where $\Sigma^\star$ is the ADC(3) self-energy, μ is the reduced mass of the $(A - 1)$-body system plus the ejected nucleon, and $\tilde{I}(k)$ represents the Fourier-Hankel transform of Eq. (1). We perform computations using the NNLO$_{\rm sat}$ interaction because of its good saturation properties [31]. Both radii and binding energies are known to be well reproduced for the oxygen chain nuclei used in this analysis [32], allowing for a meaningful comparison with reactions from Woods-Saxon–based calculations.

We show the results for (p, pN) quasifree cross sections using overlap functions obtained with (a) the SCGF formalism

with the chiral NNLO$_{\rm sat}$ interaction, denoted $I_{\rm GF}(r)$; and (b) single-particle wave functions, $u_{\rm WS}(r)$ generated in a potential model, herewith denoted WS. The WS radii and diffuseness parameters were taken as $R = 1.2A^{1/3}$ fm and $a = 0.65$ fm, respectively. A homogeneously charged sphere with radius R was used to generate the Coulomb potential. In case (a) the spectroscopic factors given by $S_{\rm GF} = \int dr I_{\rm GF}^2(r)$ are computed directly from the associated SCGF propagators. In case (b) the WS model cannot predict the normalization of the overlap functions, hence only empirical spectroscopic factors ($S_{\rm WS}^{\rm emp}$) can be obtained by calculating the quasifree cross sections and comparing them to the experimental data. Our comparison of the cross-section calculations will follow the reaction theory developed in Ref. [21] keeping all other input parameters the same, such as separation energies and nuclear densities.

In Table I we list a series of properties of proton (neutron) knockout reactions for 350-MeV protons in inverse kinematics and for oxygen isotopes incident on ^{9}Be targets at 350 MeV/nucleon. A selected set of neutron and proton states in oxygen isotopes was chosen. In some cases, we included more than one final state for the same nucleus and partial wave removal, corresponding to different excitations of the residual nucleus (hence, different E_B). These are computed as distinct correlated $(A - 1)$-nucleon states by the SCGF, while we can only assume the same mean-field orbit for all of them when using the WS. The shell model explains this fragmentation of the spectrum very well but it falls short of providing microscopic information on the differences between their radial overlaps, similarly to the WS. The last column in Table I lists the spectroscopic factors, as computed from the *ab initio* SCGF. To simplify the comparison and focus on the ANC contribution, in this study we keep all GF overlap and WS functions normalized to 1, i.e., the cross sections have not been multiplied by the spectroscopic factors S_{lj}. In the asymptotic limit (where the nuclear force is vanishingly small), the radial part of the WS wave function and GF overlaps can be expressed in terms of the Whittaker function and a corresponding ANC, C_{lj}, can be deduced.

The r.m.s. radii of the GF wave functions are slightly larger than those of the WS wave functions. There seems to be a one-to-one correspondence of this behavior with the quasifree (p, pN) cross sections, which are larger for the GF wave functions. The only exception is the $s_{1/2}$ state in ^{15}N (fourth row in Table I), which does not have dominant single-particle character and cannot be directly associated either to a $1s_{1/2}$ or to a $2s_{1/2}$ orbit. The increase in the cross sections with the r.m.s. radii of the wave function is also clearly visible for the additional three cases (one for ^{16}O and two others for ^{22}O), where the parameters of the WS potential were adjusted to reproduce the same binding energies and same r.m.s. radii as the GF wave functions. The comparison between the cross sections for WS and GF wave functions improves, but very noticeable differences remain, pointing again to the fact that both quasifree scattering and knockout reaction mechanisms depend on the details of the wave functions. Spectroscopic factors similar to those listed in Table I were used in Ref. [22] and shown to reproduce the data rather well. It is also noteworthy that in a few cases the ANC values are very different

---

[1]Spectroscopic factors are often labeled $C^2\tilde{S}$ in shell-model and reaction theory. $\tilde{S}$ represents the quenching of strength due to internucleon correlations, while C^2 is a Clebsh-Gordan coefficient that accounts for partial occupation of orbits. Here, we follow the convention from the *ab initio* community using $S \equiv C^2\tilde{S}$, to avoid confusion between ANCs and Clebsh-Gordans.

TABLE I. Separation energies, E_B, root mean square radii of the overlap wave function, $\langle r^2 \rangle^{1/2}$, asymptotic normalization coefficients, (p, pN) quasifree cross sections, σ_{qf}, and nucleon knockout cross sections, σ_{ko}, with ^{9}Be targets, for 350 MeV/nucleon oxygen projectiles. "WS" denotes wave functions calculated with a potential model (Woods-Saxon) and "GF" denotes many-body *ab initio* overlap functions from the self-consistent Green's function method. In a few cases we generated two different WS orbits, with the second choice constrained to reproduce the same radii as the GF. Different final states are distinguished by their separation energy, E_B. The first column indicates the target isotope and the mean-field WS orbit that could be tentatively associated with the transferred nucleon. S_{GF} values are theoretical spectroscopic factors predicted by the self-consistent GF; all other results employ overlap functions normalized to unity.

Nucleus (state)	E_B (MeV)	$\langle r^2 \rangle^{1/2}_{WS}$ (fm)	$\langle r^2 \rangle^{1/2}_{GF}$ (fm)	C_{WS} (fm$^{-1/2}$)	C_{GF} (fm$^{-1/2}$)	σ^{WS}_{qf} (mb)	σ^{GF}_{qf} (mb)	σ^{WS}_{ko} (mb)	σ^{GF}_{ko} (mb)	S_{GF}
^{14}O ($\pi 1p_{3/2}$)	8.877	2.836	2.961	6.665	7.060	20.72	21.28	26.28	28.15	0.548
^{14}O ($\pi 1p_{1/2}$)	6.181	2.991	3.160	4.872	5.401	21.08	16.89	28.61	31.33	0.760
^{14}O ($\nu 1p_{3/2}$)	21.33	2.513	2.722	11.39	14.64	30.55	32.80	21.13	23.92	0.773
^{16}O ($\pi s_{1/2}$)	15.89	2.295	2.233	13.06	13.81	7.870	7.696	16.97	15.81	0.074
^{16}O ($\pi 1p_{3/2}$)	17.43	2.612	2.832	15.29	18.27	17.41	18.58	19.83	22.70	0.805
^{16}O ($\pi 1p_{1/2}$)	10.65	2.816	3.077	8.624	10.70	9.094	9.913	22.54	26.29	0.794
		3.077		11.22		9.625		25.24		
^{16}O ($\nu 1p_{3/2}$)	20.71	2.580	2.807	11.96	13.88	27.88	30.26	18.81	21.66	0.801
^{16}O ($\nu 1p_{1/2}$)	13.83	2.767	3.032	6.684	7.578	14.64	16.47	21.20	24.89	0.790
^{22}O ($\pi 1p_{3/2}$)	29.26	2.554	2.884	43.74	63.52	14.37	17.08	13.07	14.50	0.274
		2.884		75.87		15.47		15.72		
^{22}O ($\pi 1p_{3/2}$)	25.67	2.606	2.820	35.00	54.07	13.30	14.20	12.93	15.10	0.443
		2.820		49.22		15.13		14.66		
^{22}O ($\pi 1p_{1/2}$)	23.58	2.634	2.916	30.49	51.49	6.607	7.253	13.27	16.21	0.731
^{22}O ($\nu 1d_{5/2}$)	6.670	3.328	3.533	4.519	4.685	45.30	46.63	21.36	24.28	0.806
^{24}O ($\pi 1p_{3/2}$)	28.57	2.609	2.886	45.76	66.45	12.13	13.29	11.37	14.01	0.675
^{24}O ($\pi 1p_{3/2}$)	31.88	2.566	2.847	55.88	95.22	11.94	13.11	10.98	13.70	0.042
^{24}O ($\pi 1p_{1/2}$)	25.28	2.657	2.985	37.04	57.21	6.054	6.881	11.81	15.11	0.740
^{24}O ($\nu 2s_{1/2}$)	4.120	4.190	4.479	3.971	4.130	13.94	19.95	31.81	36.45	0.844
^{24}O ($\nu 1d_{5/2}$)	6.961	3.436	3.557	2.056	2.106	40.53	41.95	19.51	21.11	0.832

between the WS and the GF wave functions. In essence, *it is not necessary, or expected, that the GF wave functions reproduce the same ANC as in the WS case because they are constrained by the integral of their internal part, which can vary sensibly due to correlations.*

Earlier *ab initio* wave functions obtained from expansions in harmonic oscillator wave functions did not reproduce the large-distance behavior of the nuclear states unless the expansion ran over a very large number of oscillator shells [33–35]. A simple way to prevent unnecessary large-scale calculations was reported in Refs. [34,35] by using a procedure that replaces *ab initio* wave functions at their tails with those with appropriate asymptotic behavior such as solutions of a WS model. A fit extending to the internal part of the *ab initio* overlap functions and adequate renormalization yields appropriate values for the ANCs. In fact, it was shown in Refs. [34,35] that this procedure leads to an excellent description of cross sections and momentum distributions of proton/neutron knockout reactions with heavy targets based on overlap functions stemming from the no-core shell model. Similar issues are now fully resolved both for the no-core shell model [36] and for SCGF theories. In our case, the projection of Eq. (4) into momentum space, as discussed in Ref. [30], always yields the correct asymptotics without the need for *ad hoc* corrections.

Probing deep inside the nucleus. An exact reproduction of a Whittaker tail is irrelevant in (p, pN) reactions. To show this, in Fig. 1 we plot the overlap functions for a few selected states

from Table I. All cases are for protons except the bottom-right panel, which is for a neutron single-particle state. Solid lines represent SCGF calculations, and dashed lines Woods-Saxon potentials with parameters fitted to match the same separation energies. Evidently, the forms of the wave functions are not
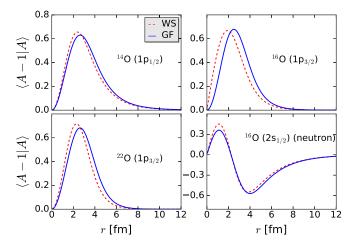

FIG. 1. Overlap functions for selected states from Table I. All cases are for protons except the bottom-right panel, which is for a neutron single-particle state. Solid lines represent calculations with the *ab initio* self-consistent Green's function (GF) method, and dashed lines Woods-Saxon (WS) potentials reproducing the same separation energies.
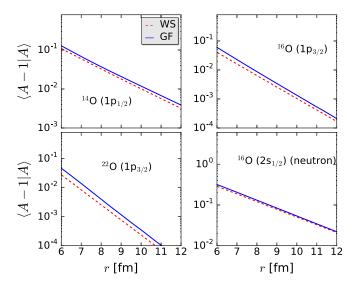
FIG. 2. Same as Fig. 1, but showing the logarithmic tail of the overlap functions.

very different, but some differences in the details are noticeable and have an impact on the r.m.s. radii and on the quasifree cross sections, as one can easily see in Table I. The cross sections can change by as much as 20%.

In Fig. 2 we show the logarithmic tails of the same wave functions as in Fig. 1. It is clear that our SCGF overlap functions possess very reasonable exponential slopes, as with the WS wave functions. Therefore, small differences in the knockout cross sections in Table I are due to the authentic modification of the height of the tails due to many-body effects stemming from the interior part of the GF overlap functions. All wave functions are normalized to unity.

Substantial differences exist in heavy-ion knockout cross sections obtained with single-particle versus many-body overlap functions. This cannot be ascribed to the asymptotic behavior of the wave functions. By simply rescaling the tails of the wave function with an ANC or a spectroscopic factor would lead to an incorrect experimental analysis, i.e., *just the ANC, or spectroscopic factor, is not enough. Full knowledge of the wave function is necessary.*
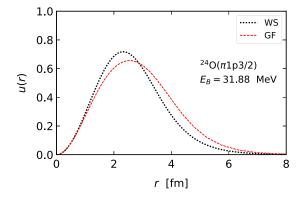

FIG. 3. Woods-Saxon (WS; dotted black line) wave function and Green's function (GF; dashed red line) overlap function for ^{24}O, $1p3/2$, $E_B = 31.88$ MeV.
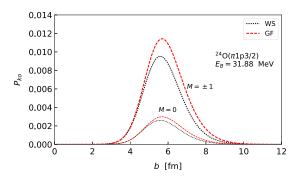

FIG. 4. Probability of removing a proton from ^{24}O, $1p3/2$, $E_B = 31.88$ MeV for Woods-Saxon (WS; dotted black line) and Green's function (GF; dashed red line) in the $M = 0$ (thin lines) and $M = \pm 1$ (thick lines) channels calculated with Eq. (5).

To clarify the latter point and show that *knockout reactions with heavy ions are also partially sensitive to details of the inner part of the wave functions*, consider the probability of one-nucleon stripping in a collision with the core (surviving spectator) having an impact parameter b with the target, while the removed nucleon has an impact parameter b_n. The stripping probability is [7]

$$P_{\text{ko}}(b) = \mathcal{S}_c(b)\langle 1 - |\mathcal{S}_n(\mathbf{b}_n)|^2\rangle$$
$$= \mathcal{S}_c(b)\int d^3r |\phi_{nlj}(\mathbf{r})|^2 (1 - |\mathcal{S}_n(\mathbf{b}_n)|^2), \quad (5)$$

where $\phi_{nlj}(\mathbf{r})$ denotes the wave function with quantum numbers nlj expressed in terms of the relative core-neutron distance $\mathbf{r}$. $\mathcal{S}_c$ ($\mathcal{S}_n$) is the scattering matrix for the core (nucleon)–target and $|\phi_{nlj}|^2$ is the probability of finding the nucleon at $\mathbf{r}$. $\mathbf{b}_n \equiv (b_n, \phi_n)$ and the intrinsic coordinate $\mathbf{r} \equiv (r, \theta, \phi)$ are related by [7]

$$b = \sqrt{r^2 \sin^2\theta + b_n^2 - 2rb_n\sin\theta\cos(\phi - \phi_n)}. \quad (6)$$
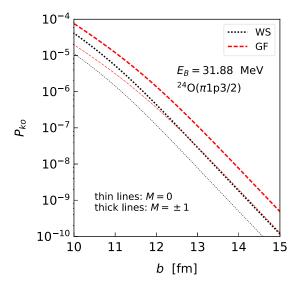

FIG. 5. Same as Fig. 4, but for very large impact parameters b, where the integrand in Eq. (5) is dominated by the tail of the wave function of the removed nucleon.
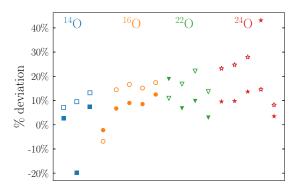
FIG. 6. Percentage deviation of cross sections using WS wave functions and GF overlaps for the 17 reactions listed in Table I for quasifree scattering (filled symbols) and knockout reactions (open symbols). Cross sections calculated with the GF overlaps are larger than those calculated with the WS wave functions, except for two states.

We apply Eq. (6) to obtain the heavy-ion proton knockout from ^{24}O, $1p3/2$, with $E_B = 31.88$ MeV. In Fig. 3 we compare the GF and WS wave functions, noting that while the tails are similar to a Whittaker function (only seen on a logarithmic scale), there are visible differences in their overall shapes. The calculated proton stripping probabilities from Eq. (5) are shown in Fig. 4. They are larger for the GF wave functions, yielding larger cross sections, as expected upon inspection of Table I.

A simple question arises: Do the heavy-ion knockout cross sections scale with the squares of the ANCs? The answer is negative. The respective ANCs scale as $(C_{GF}/C_{WS})^2 \sim 3$, whereas the cross sections scale as $\sigma_{ko}^{GF}/\sigma_{ko}^{WS} \sim 1.25$. This intriguing difference is best understood if the stripping probability is plotted logarithmically for large b. This is shown in Fig. 5. While at very large distances, the probability seems as if it scales with a single factor (the ratio between the ANCs), at lower but still large impact parameters it visibly differs from simple scaling. This result is understood by considering the stripping probability in Eq. (5). Even for large b, when the core and the target pass by as much as 10 fm apart, the inner parts of the wave function are still probed because the integrand is too small to make substantial contributions to the probability if $b_n \gg 1$, as $1 - |S_n|^2$ decreases rapidly. We have observed the same behavior for all the cases listed in Table I.

The imprints of the details of the many-body overlap functions are summarized in Fig. 6 for the 17 reactions listed in Table I. The horizontal scale is a list of the reactions in Table I

from top to bottom of the table. The vertical scale represents $(\sigma_{GF} - \sigma_{WS})/\sigma_{WS}$ as a percentage for (p, pN) reactions. Except for two cases, the quasifree cross sections calculated with the GF overlaps are larger than those calculated with the WS wave functions. The squares (diamonds) [circles] {stars} represent these quantities for 350 MeV/nucleon ^{14}O (^{16}O) [^{22}O] {^{24}O} projectiles. It is evident that the results change appreciably with a different form of the internal part of the overlap functions. Figure 6 also demonstrates that variations with respect to the overlap functions are smaller in the (p, pN) case (filled symbols). This is due to the capability of this reaction mechanism to better probe the internal part of the nucleus.

Conclusions. In contrast to a commonly considered idea, *both* heavy-ion knockout reactions and (p, pN) reactions are sensitive to the internal details of the overlap wave function and place strong constraints on the coordinate dependence of the many-body wave functions.

An accurate experimental analysis ideally requires not only the input of an accurately determined overlap function from many-body computations, but also a direct comparison among possible predictions, so that one can assess the extent of the model dependence for the inferred spectroscopic factors. The latter task requires particular attention since a good reproduction of nuclear binding energies and radii is a fundamental constraint but only a fraction of currently available *ab initio* Hamiltonians offer satisfactory saturation properties [37–39]. While this poses a more difficult task for the study of single-particle configurations with heavy-ion knockout and (p, pN) reactions, it also provides opportunities for a better and more profound understanding of many-body configurations and their single-particle overlaps.

In view of the recent advances in experimental facilities and detection techniques, it is suggested that heavy-ion knockout and (p, pN) reactions be analyzed using a consistent many-body model, because they are a formidable tool to extend our knowledge in nuclear spectroscopy only when many-body correlations are considered in the analysis.

[1] R. Anne *et al.*, Phys. Lett. B **250**, 19 (1990).

[2] K. Riisager *et al.*, Nucl. Phys. A **540**, 365 (1992).

[3] N. A. Orr, N. Anantaraman, S. M. Austin, C. A. Bertulani, K. Hanold, J. H. Kelley, D. J. Morrissey, B. M. Sherrill, G. A. Souliotis, M. Thoennessen, J. S. Winfield, and J. A. Winger, Phys. Rev. Lett. **69**, 2050 (1992).

[4] C. A. Bertulani and K. W. McVoy, Phys. Rev. C **46**, 2638 (1992).

[5] H. Esbensen, Phys. Rev. C **53**, 2007 (1996).

[6] K. Hencken, G. Bertsch, and H. Esbensen, Phys. Rev. C **54**, 3043 (1996).

[7] C. A. Bertulani and P. G. Hansen, Phys. Rev. C **70**, 034609 (2004).

[8] C. Bertulani and A. Gade, Comput. Phys. Commun. **175**, 372 (2006).

[9] P. G. Hansen, Phys. Rev. Lett. **77**, 1016 (1996).

[10] C. Hebborn and P. Capel, Phys. Rev. C **100**, 054607 (2019).

[11] A. Bonaccorso, R. J. Charity, R. Kumar, and G. Salvioni, AIP Conf. Proc. **1645**, 30 (2015).

[12] T. Aumann *et al.*, Prog. Part. Nucl. Phys. **118**, 103847 (2021).

[13] T. Aumann, A. Navin, D. P. Balamuth, D. Bazin, B. Blank, B. A. Brown, J. E. Bush, J. A. Caggiano, B. Davids, T. Glasmacher, V. Guimaraes, P. G. Hansen, R. W. Ibbotson, D. Karnes, J. J. Kolata, V. Maddalena, B. Pritychenko, H. Scheit, B. M. Sherrill, and J. A. Tostevin, Phys. Rev. Lett. **84**, 35 (2000).

[14] S. Boffi, C. Giusti, F. d. Pacati, and M. Radici, *Electromagnetic Response of Atomic Nuclei*, Oxford Studies in Nuclear Physics, Vol. 20 (Clarendon, Oxford, 1996).

[15] P. G. Hansen and J. A. Tostevin, Annu. Rev. Nucl. Part. Sci. **53**, 219 (2003).

[16] C. Barbieri, Phys. Rev. Lett. **103**, 202502 (2009).

[17] E. Caurier, G. Martínez-Pinedo, F. Nowack, A. Poves, and A. P. Zuker, Rev. Mod. Phys. **77**, 427 (2005).

[18] A. Gade, P. Adrich, D. Bazin, M. D. Bowen, B. A. Brown, C. M. Campbell, J. M. Cook, T. Glasmacher, P. G. Hansen, K. Hosier, S. McDaniel, D. McGlinchery, A. Obertelli, K. Siwek, L. A. Riley, J. A. Tostevin, and D. Weisshaar, Phys. Rev. C **77**, 044306 (2008).

[19] A. M. Mukhamedzhanov and N. K. Timofeyuk, Sov. J. Exp. Theor. Phys. Lett. **51**, 282 (1990).

[20] V. Panin *et al.*, Phys. Lett. B **753**, 204 (2016).

[21] T. Aumann, C. A. Bertulani, and J. Ryckebusch, Phys. Rev. C **88**, 064610 (2013).

[22] L. Atar *et al.* (R³B Collaboration), Phys. Rev. Lett. **120**, 052501 (2018).

[23] S. Kawase *et al.*, Prog. Theor. Exp. Phys. **2018**, 021D01 (2018).

[24] K. Ogata, K. Yoshida, and K. Minomo, Phys. Rev. C **92**, 034616 (2015).

[25] A. M. Moro, Phys. Rev. C **92**, 044605 (2015).

[26] A. Cipollone, C. Barbieri, and P. Navrátil, Phys. Rev. C **92**, 014306 (2015).

[27] A. Carbone, A. Cipollone, C. Barbieri, A. Rios, and A. Polls, Phys. Rev. C **88**, 054326 (2013).

[28] J. Schirmer, L. S. Cederbaum, and O. Walter, Phys. Rev. A **28**, 1237 (1983).

[29] C. Barbieri and A. Carbone, in *An Advanced Course in Computational Nuclear Physics*, edited by N. Hjorth-Jensen, M. P. Lombardo, and U. van Kolck, Lecture Notes in Physics Vol. 936 (Springer, Berlin, 2016), p. 571.

[30] A. Idini, C. Barbieri, and P. Navrátil, Phys. Rev. Lett. **123**, 092501 (2019).

[31] A. Ekström, G. R. Jansen, K. A. Wendt, G. Hagen, T. Papenbrock, B. D. Carlsson, C. Forssén, M. Hjorth-Jensen, P. Navrátil, and W. Nazarewicz, Phys. Rev. C **91**, 051301(R) (2015).

[32] V. Lapoux, V. Somà, C. Barbieri, H. Hergert, J. D. Holt, and S. R. Stroberg, Phys. Rev. Lett. **117**, 052501 (2016).

[33] F. Flavigny, A. Gillibert, L. Nalpas, A. Obertelli, N. Keeley, C. Barbieri, D. Beaumel, S. Boissinot, G. Burgunder, A. Cipollone, A. Corsi, J. Gibelin, S. Giron, J. Guillot, F. Hammache, V. Lapoux, A. Matta, E. C. Pollacco, R. Raabe, M. Rejmund, N. deSereville, A. Shrivastava, A. Signoracci, and Y. Utsuno, Phys. Rev. Lett. **110**, 122503 (2013).

[34] P. Navrátil, C. Bertulani, and E. Caurier, Phys. Lett. B **634**, 191 (2006).

[35] P. Navrátil, C. A. Bertulani, and E. Caurier, Phys. Rev. C **73**, 065801 (2006).

[36] S. Baroni, P. Navrátil, and S. Quaglioni, Phys. Rev. C **87**, 034326 (2013).

[37] M. Piarulli and I. Tews, Front. Phys. **7**, 245 (2020).

[38] E. Epelbaum, H. Krebs, and P. Reinert, Front. Phys. **8**, 98 (2020).

[39] A. Ekström, Front. Phys. **8**, 29 (2020).